

Multispecies reactive tracer test in an aquifer with spatially variable chemical conditions, Cape Cod, Massachusetts: Dispersive transport of bromide and nickel

Kathryn M. Hess

U.S. Geological Survey, Northborough, Massachusetts, USA

James A. Davis, Douglas B. Kent, and Jennifer A. Coston

U.S. Geological Survey, Menlo Park, California, USA

Received 10 September 2001; revised 9 April 2002; accepted 12 April 2002; published 31 August 2002.

[1] Dispersive transport of groundwater solutes was investigated as part of a multispecies reactive tracer test conducted under spatially variable chemical conditions in an unconfined, sewage-contaminated sand and gravel aquifer on Cape Cod, Massachusetts. Transport of the nonreactive tracer bromide (Br) reflected physical and hydrologic processes. Transport of the reactive tracer nickel (Ni) complexed with an organic ligand (NiEDTA) varied in response to pH and other chemical conditions within the aquifer. A loss of about 14% of the Ni mass was calculated from the distribution of tracers through time. This loss is consistent with reversible adsorption of NiEDTA onto the iron and aluminum oxyhydroxide coatings on the aquifer sediments. The Ni consistently lagged behind Br with a calculated retardation coefficient of 1.2. Longitudinal dispersivities reached constant values of 2.2 and 1.1 m for Br and Ni, respectively, by at least 69 m of travel. The smaller dispersivity for Ni possibly was due to nonlinear or spatially variant adsorption of NiEDTA. In the upper, uncontaminated zone of the aquifer, longitudinal dispersion of Ni was greater than that of Br early in the test as a result of reversible adsorption of NiEDTA. In general, transverse dispersivities were much smaller (horizontal: $1.4\text{--}1.5 \times 10^{-2}$ m; vertical: $0.5\text{--}3.8 \times 10^{-3}$ m) than the longitudinal dispersivities. The Br results are similar to those from a test conducted eight years earlier, suggesting that transport parameters are spatially stationary within the aquifer at the scale of 300 m covered by the spatially overlapping tests. A significant difference between the two tests was the travel distance (69 and 26 m) needed to reach a constant longitudinal dispersivity. **INDEX TERMS:** 1829 Hydrology: Groundwater hydrology; 1831 Hydrology: Groundwater quality; 1832 Hydrology: Groundwater transport; 5139 Physical Properties of Rocks: Transport properties; **KEYWORDS:** dispersion, Cape Cod, tracer test, transport, groundwater

1. Introduction

[2] A groundwater tracer test was initiated in 1993 at the U.S. Geological Survey's Toxics Substances Hydrology Research site on Cape Cod, Massachusetts (Figure 1), to investigate the fate and transport of reactive species compared to that of a conservative solute under spatially variable chemical conditions [Davis *et al.*, 2000, 2001a, 2001b]. Background chemical conditions, such as pH, dissolved oxygen, and concentrations of major ions and complexing ligands, vary spatially at many contaminated sites. Physical and chemical heterogeneity within an aquifer contributes to the complex transport behavior of many contaminants [Tompson and Jackson, 1996]. Reactive transport models that couple chemical reactions with advection-dispersion equations describing groundwater flow [Engesgaard and Traberger, 1996; Yeh and Salvage, 1995; Parkhurst, 1995] can be used advantageously to model contaminant transport. Detailed field experiments are needed to provide data sets for

calibration of these models. The purpose of the experiment partially described here was to provide such a chemically complex data set.

[3] Transport behaviors of the two tracers reported here, bromide (Br) and nickel (Ni), were expected to differ. Br, an anion, was the conservative, nonreactive tracer, whereas Ni, a divalent cation, was injected as a complex with the organic ligand EDTA (ethylenediaminetetraacetic acid), predominantly forming an anion, NiEDTA²⁻, and minor amounts of other anionic compounds. The term NiEDTA will be used for the group of complexed compounds. NiEDTA weakly adsorbs onto the iron and aluminum oxyhydroxide coatings on the aquifer sediments [Nowack and Sigg, 1996]. NiEDTA retardation was expected to vary in different vertical zones of the aquifer in response to vertical variability in pH and in concentrations of anions that compete for sorption sites. This paper compares the manner in which the two tracers traveled and dispersed through the aquifer.

[4] Through the results of this test, we revisit issues of macrodispersion of solutes that were addressed in a well-documented tracer test conducted eight years earlier (1985–1988) in the same aquifer [LeBlanc *et al.*, 1991; Garabe-

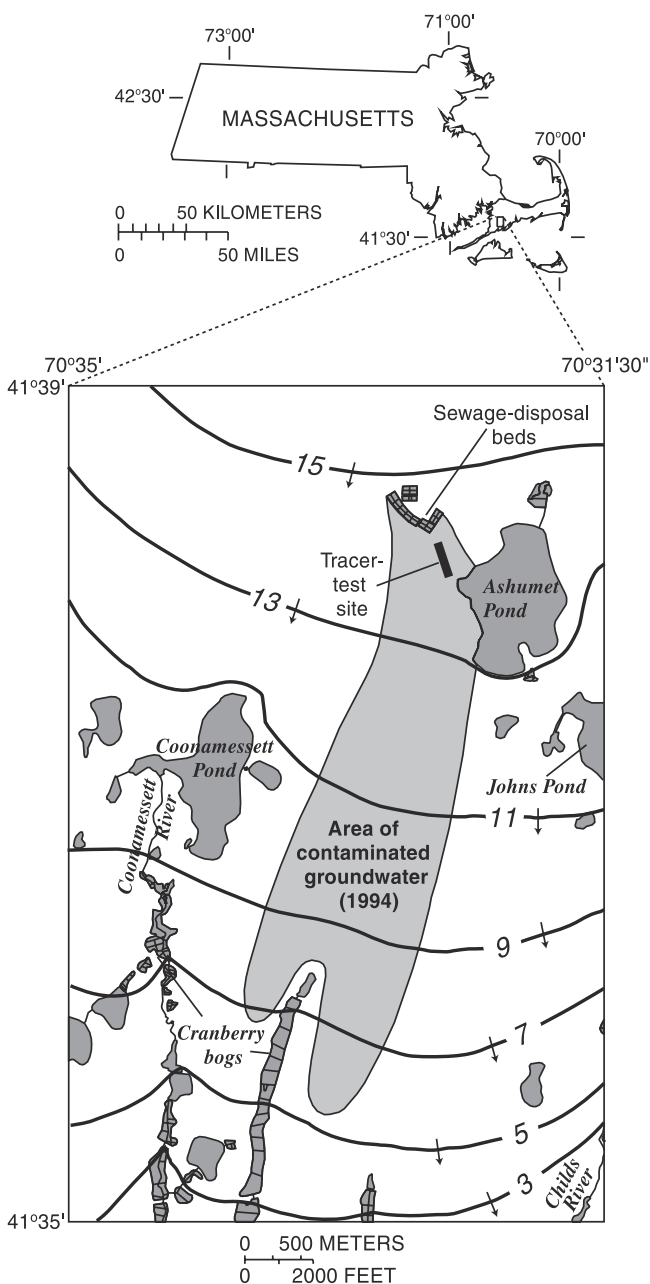


Figure 1. Location of tracer test site, area of contaminated groundwater (1994), and water table contours (1993), western Cape Cod, Massachusetts. Arrows indicate general direction of groundwater flow.

dian et al., 1991]. In the 1985–1988 test, an injection of Br was monitored for 511 days as it traveled over 200 m through the aquifer. The transport parameters obtained from that tracer test were compared with those calculated in a companion study [Hess et al., 1992] in which the variability of hydraulic conductivity in the aquifer was quantified. These earlier field and laboratory experiments provided a field trial of stochastic transport theories, such as those of Gelhar and Axness [1983], that relate macrodispersion to the statistical properties of the spatial distribution of physical heterogeneity within the aquifer. Only a few controlled field experiments have been conducted with a travel dis-

tance of 100 m or greater; the tests at Base Borden, Ontario [Mackay et al., 1986], and Columbus, Mississippi [Boggs et al., 1992; MacIntyre et al., 1993], are some of the best known. In this paper we evaluate the reproducibility of this type of large-scale field experiment and examine the spatial stationarity of transport properties within the aquifer.

2. Tracer Injection

[5] The test began on April 21, 1993, with an injection of 9884 L of groundwater into which the nonreactive tracer Br (3.43 mmol/L) and the reactive tracer Ni (0.256 mmol/L) complexed with EDTA (1.112 mmol/L) had been added. Detailed descriptions of the injectate, including the tracers not described here (chromium (VI), and zinc-, lead- and copper-EDTA), and the injection process are presented by Davis et al. [2000, 2001a, 2001b]. The tracer Br was expected to travel through the aquifer without reacting with the sediments; conservative, nonreactive transport of Br had been observed previously in many field experiments conducted at this site [Garabedian et al., 1991; Harvey and Garabedian, 1991; Smith et al., 1991; Kent et al., 1994]. The 1993 injection occurred in the same aquifer 43 m downgradient from the 1985 injection site [LeBlanc et al., 1991]. The regions of the aquifer traversed in the two tests were different, but there was some spatial overlap.

[6] The shallow, unconfined aquifer is composed of interfingering sand and gravel lenses deposited in a glacial outwash plain [Oldale and Barlow, 1986; Masterson et al., 1997]. Less than 1% of the sediments in the aquifer are silt-sized or finer grained [Barber et al., 1992]. The coarse-grained deposits are about 50 m thick at the tracer test site. The average hydraulic conductivity is about 0.1 cm/s [Hess et al., 1992]. Visual inspection of exposed sediment [see LeBlanc et al., 1991, Figure 3] and results of *in situ* and laboratory hydraulic tests [Wolf et al., 1991; Hess et al., 1992] indicate a moderate degree of physical heterogeneity within the aquifer sediments; hydraulic conductivities vary over about one order of magnitude. Variability in the hydraulic-conductivity distribution is also suggested by the variable transport velocities observed in numerous small-scale tracer tests conducted at the site [e.g., see Harvey and Garabedian, 1991; Smith et al., 1991; Kent et al., 1994]. On the basis of calculations that use the stochastic transport theories of Gelhar and Axness [1983], the small-scale variability in hydraulic conductivity observed at the site is sufficient to account for the scale of longitudinal macrodispersion observed in the earlier tracer test [Garabedian et al., 1991; Hess et al., 1992].

[7] Anion and cation adsorptive properties of the aquifer sediments are controlled by iron- and aluminum-bearing coatings on the mineral grains [Coston et al., 1995]. Chemical heterogeneity in the adsorptive properties of the aquifer sediments is consistent with the observed variability in the quantity and composition of coatings [Fuller et al., 1996].

[8] The chemical composition of the groundwater at the tracer test site varied vertically due to a plume of contaminated groundwater (Figure 1) emanating from a sewage wastewater treatment and disposal facility 250 m upgradient of the tracer injection site [LeBlanc, 1984; Walter et al., 1996]. The upper zone of the aquifer had pristine groundwater, characterized by low pH (5–5.5) and low ionic concentrations (specific conductance, <100 $\mu\text{S}/\text{cm}$; phosphate, <5 $\mu\text{mol}/\text{L}$). The deeper,

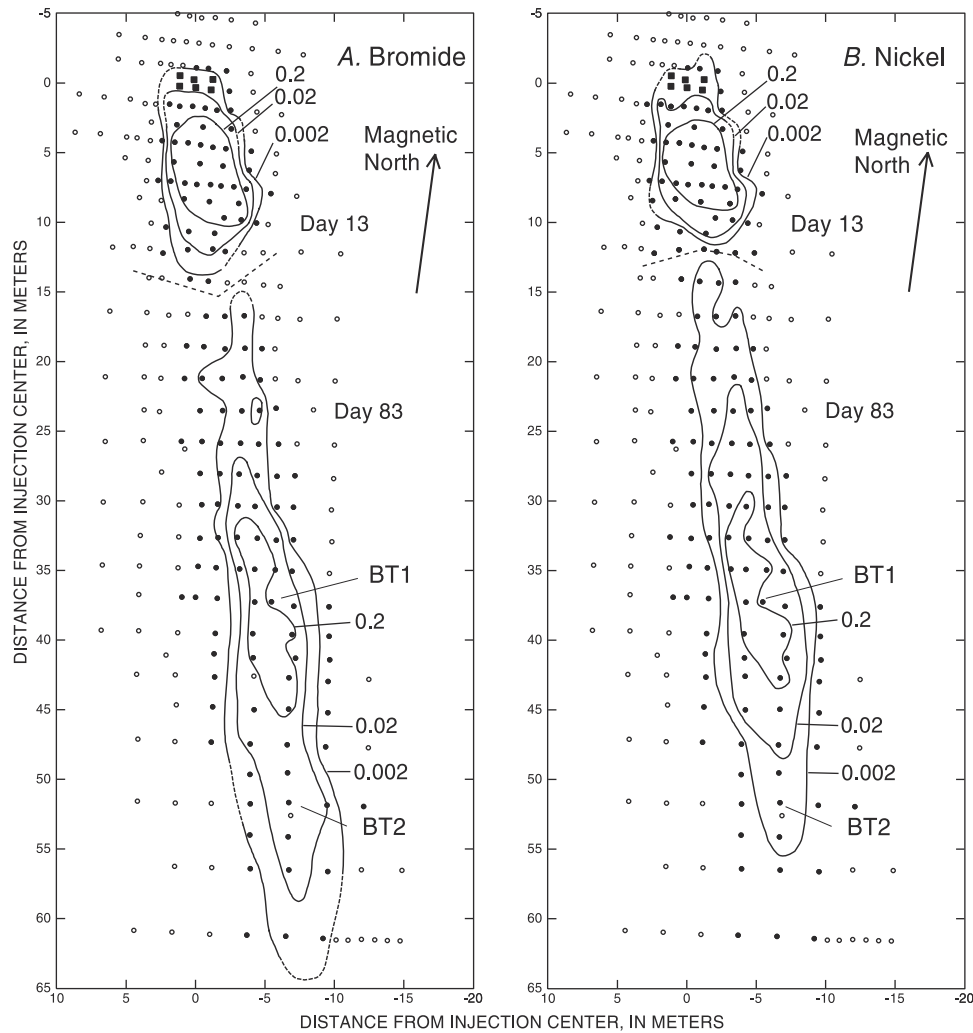


Figure 2. Distributions of maximum (a) bromide and (b) nickel concentrations observed 13 and 83 days after the injection (dashes where inferred). Concentrations are normalized relative to the injection concentrations. Also shown are locations of multilevel samplers (MLS) available for sampling during the tracer test (open circles), MLS sampled at 13 and 83 days (solid circles), the six injection MLS (solid squares), and the two breakthrough curve MLS (BT1 and BT2).

sewage-contaminated groundwater was characterized by higher pH (6–6.5) and higher ionic concentrations (specific conductance, $>300 \mu\text{S}/\text{cm}$; phosphate, $15\text{--}160 \mu\text{mol}/\text{L}$). Between the pristine and contaminated zones was a transition zone through which the water chemistry changed considerably over a vertical distance of only 1 to 2 m. In the transition zone, contaminant levels were high enough and pH levels were low enough that dissolved zinc from the disposed sewage had traveled as far downgradient as the middle of the tracer test site [Rea *et al.*, 1991; Kent *et al.*, 2000]. Detailed characterization of the chemical zones is presented elsewhere [see Davis *et al.*, 2000, Figure 4].

[9] The tracers were injected into the aquifer across all three chemical zones. Approximately half of the tracer mass (53.5%) was injected into the transition zone; significant mass also was injected into the pristine (17.8%) and contaminated (28.7%) zones.

[10] Transport of the injected tracers through the aquifer was monitored by collecting groundwater samples at 15-port multilevel samplers (MLS) downgradient from the injection site. Two sampling strategies were used. With the first

strategy, samples were collected every one to three days from two MLS located 37 and 52 m downgradient (BT1 and BT2; Figure 2). This frequent sampling provided detailed breakthrough curves for each port on the two MLS. The breakthrough curve data was collected for the purpose of assessing the vertical variability of the local velocity field and of the geochemical properties within the aquifer. The second sampling strategy was to obtain monthly samples from all MLS ports within the region occupied by the tracers (Figure 2). Between 650 and 1,300 samples were taken over 2 to 3 days during each of the nine monthly synoptic sampling rounds that occurred between 13 and 314 days following the injection. These synoptic sampling rounds defined the three-dimensional distribution of tracers through time. More details on the sampling strategies and analytical methods are given by Davis *et al.* [2000, 2001a, 2001b].

3. Tracer Transport

[11] In contrast to Br, Ni was expected to react chemically with the aquifer sediments as it traveled through the

Table 1. Tracer Cloud Dimensions at 0, 13, 83, and 210 Days After the Tracer Injection on 21 April 1993, Cape Cod, Massachusetts^a

Tracer Dimension, m	Days After Injection			
	0	13	83	210
Bromide				
Longitudinal length	1.8	15	50	85
Transverse horizontal width	4	8	8	9
Vertical extent	3.5	4	6.5	6.5
Nickel				
Longitudinal length	1.8	13	43	70
Transverse horizontal width	4	8	8	11
Vertical extent	3.5	4	6	5

^aThe initial dimensions are calculated from the injection volume and the concentration distribution at the injection multilevel samplers one day after the injection. The later dimensions are derived from interpretations (maps and cross sections) of the monthly synoptic sampling data (see the 0.002 relative concentration contours on Figures 2 and 3, for example).

aquifer. Experimental measurements made throughout the tracer test demonstrated that Ni was transported exclusively as NiEDTA complexes [Davis *et al.*, 2000, 2001b]. Two primary chemical processes likely controlled the transport of NiEDTA: 1) exchange of iron (Fe(III)) for nickel in the EDTA complex, followed immediately by adsorption of the free Ni cation; and 2) reversible adsorption of the NiEDTA anion onto the iron- and aluminum-bearing coatings on the quartz-dominated aquifer sediments. Ni had the lowest affinity for exchange with Fe(III) of the four divalent metals injected as EDTA complexes, and significant dilution of the tracer cloud would be needed for the Ni exchange reaction to proceed under ambient conditions in the aquifer, according to thermodynamic modeling [Davis *et al.*, 2000, 2001b]. Adsorption of the specific injected metal-EDTA complexes, however, was not expected to differ because their affinities to adsorb onto the iron- and aluminum-bearing coatings did not differ significantly. Therefore, the exchange of Fe(III) for Ni in the EDTA complex was expected to be minimal except at the edges of the tracer cloud where significant dilution would occur; reversible adsorption of NiEDTA was expected to dominate.

[12] Adsorption of the negatively charged NiEDTA complexes was expected to increase as pH decreased [Nowak and Sigg, 1996]. In addition, NiEDTA was expected to compete with phosphate and other anions in the sewage-contaminated groundwater for adsorption sites, as Stollenwerk [1995] observed in the previous tracer test at this site, in which the reactive tracer molybdate competed with phosphate. Thus the transport of Ni was expected to vary with depth in this aquifer because of the increase in pH and in concentrations of competing anions, especially phosphate, with increasing depth.

[13] The movement and spread of Br and Ni were monitored for 237 and 314 days after injection, respectively, prior to the leading edge of each tracer cloud traveling beyond the instrumented region of the aquifer. The mapped distributions of maximum Br and Ni after 13 and 83 days of transport are shown in Figure 2. With time, the tracer clouds greatly lengthened in the direction of transport; the spread of the tracers perpendicular to the flow was much less. The dimensions of the tracer cloud, as

defined by the 0.002 relative concentration (C/C_0) contour, are reported in Table 1 for several synoptic sampling rounds. At 83 days, the leading edge of the Ni tracer trailed the leading edge of the Br tracer (Figure 2). Later, the spatial separation between the two tracers increased as the transport of Ni was retarded relative to Br.

[14] The tracer clouds are well defined in the vertical direction because of the small distance between sampling ports along each MLS (0.25 to 0.76 m). By 83 days, the Br tracer cloud had developed an asymmetrical vertical distribution with the leading edge traveling high in the aquifer relative to the trailing edge (Figure 3a). The asymmetry likely is due to variability in the flow velocity resulting from local variability in hydraulic conductivity. The asymmetry may also result from the tracer cloud's proximity to the water table. Theoretically, horizontal velocities are higher near the water table to accommodate the incoming recharge, although this increased velocity is usually not measurable. Local heterogeneity in hydraulic conductivity also may account for part of the vertical spreading of the tracers, which is apparent when comparing the Br cloud distributions at 13 and 83 days (Figure 3a). Some tracer remained high in the aquifer in the more transmissive layers and the rest of the tracer spread downward because of density-driven sinking [LeBlanc and Celia, 1996; Zhang *et al.*, 1998].

[15] The Ni cloud (Figure 3b) retained a fairly symmetric vertical form as compared to the Br cloud (Figure 3a). Transport of NiEDTA was more retarded near the water table in the uncontaminated pristine zone, where pH and competition for adsorption sites were low [Davis *et al.*, 2000, 2001a], and less retarded in the lower contaminated zone, where pH and competition were higher. This difference in chemical conditions resulted in a vertical distribution of Ni that masked the effects of physical heterogeneity within the aquifer that were apparent in the Br distribution.

3.1. Temporal Moment Analysis of Breakthrough Curves

[16] The tracers formed complex, three-dimensional clouds that flowed downgradient from the point of injection (Figures 2 and 3). The temporal patterns of tracer concentrations (Figure 4) that can be obtained by frequently sampling a position downgradient of the injection provide insight into the processes affecting the fate and transport of the tracers. The quantitative analysis of transport that can be applied to the resulting breakthrough curves yield only estimates of the local transport processes because the data and the analysis are only one dimensional when the processes affecting the transport of the tracer clouds are three dimensional.

[17] The Br breakthrough curves are predominantly sharp and symmetrical; the Ni curves are more broad and asymmetrical and consistently lag behind the Br curves (selected curves shown in Figure 4). The tracer concentrations were normalized by dividing by the respective injection concentration and, therefore, are unitless. The average time of each breakthrough, the width of the breakthrough curves, and the amount of mass represented by each curve vary.

[18] Local estimates of mass, velocity and longitudinal dispersivity can be obtained through temporal moments analysis of breakthrough curves; examples include break-

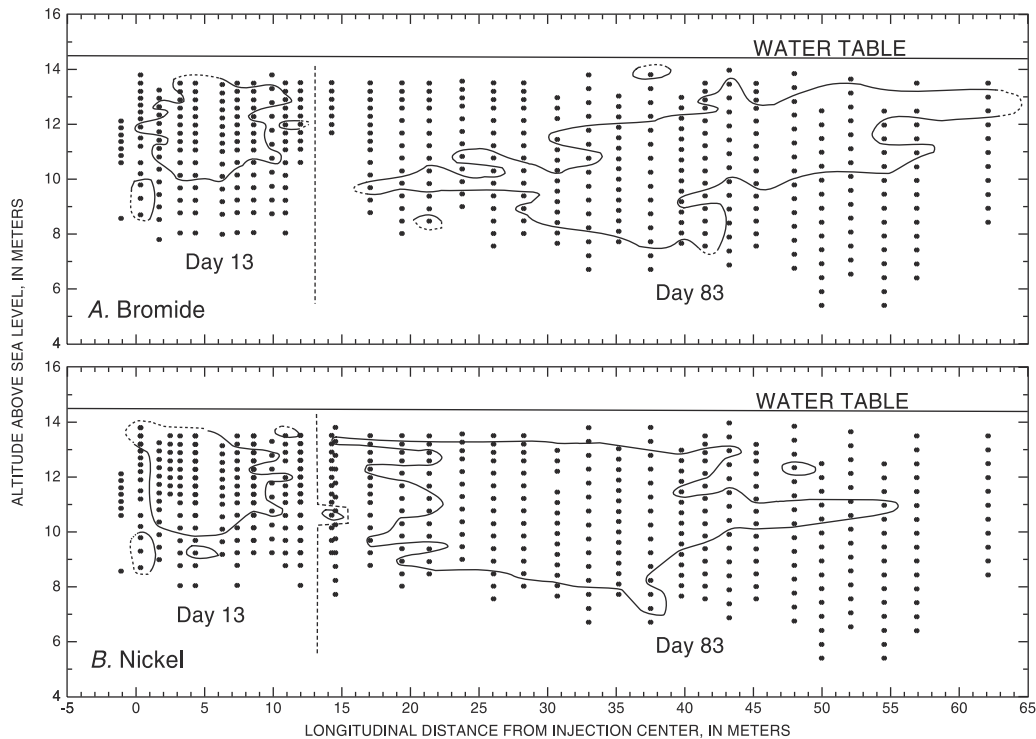


Figure 3. Longitudinal and vertical distributions of (a) bromide and (b) nickel observed 13 and 83 days after the injection. Section is aligned along the mean direction of transport. Extent of tracer is marked by the 0.002 contour of concentration normalized relative to the injection concentration.

through curves from laboratory column experiments [Valocchi, 1985] and small-scale field experiments [Kent *et al.*, 1994; Roberts *et al.*, 1986; Harvey and Garabedian, 1991]. The zeroth moment is the area under the breakthrough curve; linear trapezoidal integration is used in this analysis. The zeroth moment was divided by the average time and multiplied by the vertical interval represented by the sampling port to estimate the flux of solute mass that traveled past each sampling port. The average velocity at each port was calculated by dividing the travel distance by the estimated average time. The second moment gives a measure of the temporal spread of the breakthrough curve and can be used to estimate local longitudinal dispersivity. A simplified analysis [Harvey and Garabedian, 1991] that assumes a normal shape to the breakthrough curve was used here for Br.

[19] The mass fractions, average velocities, retardation factors, and local longitudinal dispersivities for BT2 are shown in Figure 5; similar results were obtained for BT1 breakthrough curves [Davis *et al.*, 2001a, 2001b]. Estimates of velocity and longitudinal dispersivity from breakthrough curves were assumed to be representative of the aquifer only where sufficient tracer mass had passed (mass fraction greater than or equal to 0.05; Figure 5a).

[20] The average Br velocities ranged from 0.39 to 0.66 with a median of 0.46 m/d. The transport of Ni was retarded relative to Br. At all vertical levels, Ni lagged behind Br, as reflected in the average travel time velocities (results for BT2 shown in Figure 5b). The vertical differences in adsorption of NiEDTA, because of the vertical variability in aquifer chemistry, were reflected in the range of calculated retardation factors of 1.03 to 1.26 (results for BT2

shown in Figure 5c). In general, higher retardation factors were found in the upper parts of the aquifer where pH and competition for adsorption sites were low and adsorption of NiEDTA was more extensive.

[21] The shapes of the Ni and Br breakthrough curves differ (Figure 4). This is particularly the case with curves from the upper pristine zone of the aquifer (Figure 4a) where adsorption of NiEDTA was greatest. Even though the shapes of the curves differ, the areas under the curves, and thus the mass represented by the breakthrough curves, were substantially the same, as would be expected if NiEDTA was adsorbing and then desorbing reversibly.

[22] The Br breakthrough curves provide visual examples of the effects of physical heterogeneity on solute transport. Figures 4a and 4c show breakthrough curves for Br that are remarkably similar in shape, indicating that the tracer experienced similar dispersion at the two levels within the aquifer. The obvious difference between the two peaks is that one lags significantly behind the other. This lag translates into a 0.08 m/d difference in velocity (Figure 5b). Other curves show different breakthrough shapes as well as different average travel times. The calculated dispersivities for Br quantify these different shapes and range from 0.03 to 0.51 m (results for BT2 shown in Figure 5d). The median dispersivity of 0.16 m is 1 to 2 orders of magnitude smaller than those calculated from spatial analyses of the results of large-scale experiments and several orders of magnitude smaller than those typically used in numerical simulations [Gelhar *et al.*, 1992], as is typical with longitudinal dispersivities calculated from breakthrough curves obtained in small-scale field and laboratory column tests. The breakthrough-data dispersivities, while field scale, were calcu-

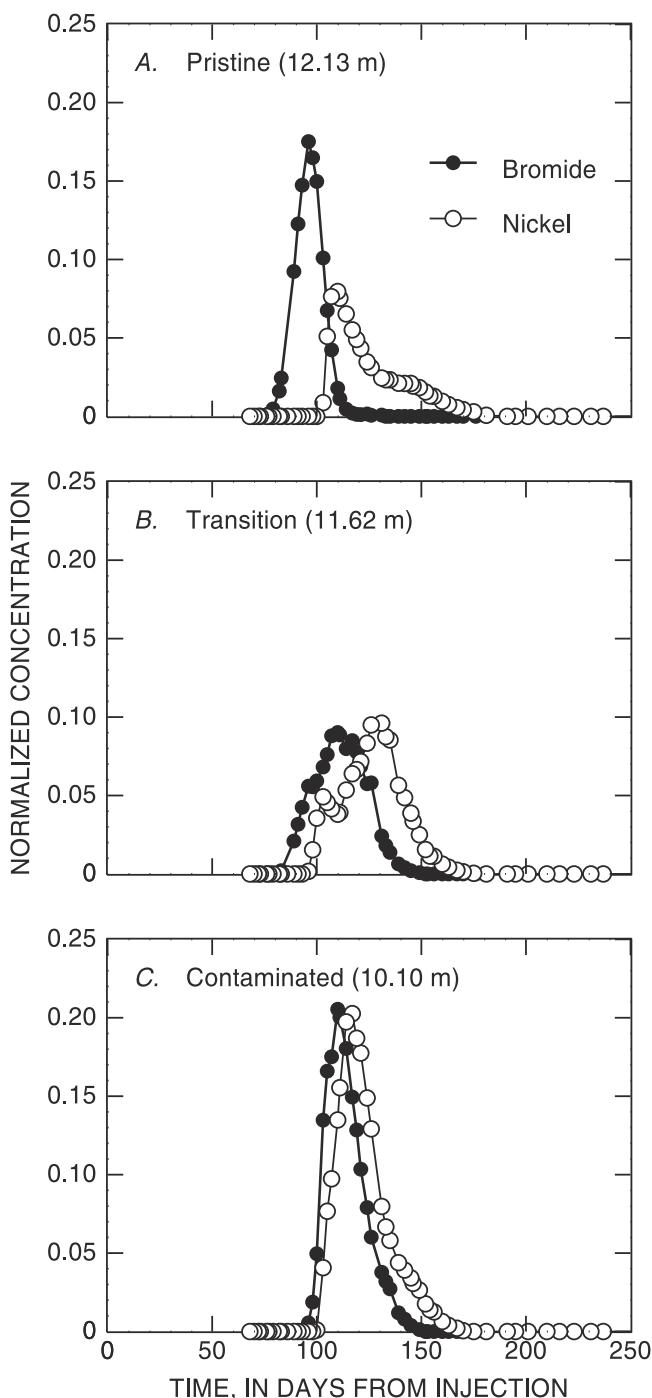


Figure 4. Bromide and nickel breakthrough curves observed at three ports on the multilevel sampler located 52 m downgradient of the center of the injection (BT2). Concentrations are normalized relative to the injection concentration. The location of BT2 is shown in Figure 2. Altitudes of ports given in meters above sea level.

lated only over tens of meters of transport. They should not be applied to larger field scales, such as the scale of a typical contaminant plume. The primary value of these estimated dispersivities is in illustrating the vertical variability in dispersion that can be observed in this type of sand and gravel aquifer.

3.2. Spatial Moment Analysis of Synoptic Data

[23] The synoptic data were analyzed using the spatial moment methods that were applied to data collected during the 1985–1988 tracer test [Garabedian *et al.*, 1991]. In general, these methods employ linear, trapezoidal interpolation vertically between sampling ports on the MLS and planar triangulation methods for areal integration; see Garabedian *et al.* [1988] and Davis *et al.* [2001a] for details on this method. The spatial moment analysis yields estimates of the solute mass, the location of the center of mass, and the variances of the solute distribution at specific points in time. Estimates of dispersivities can be made from the changes in calculated variances over time.

3.2.1. Calculated mass

[24] The zeroth moment estimates the total mass within the tracer cloud at the time of the synoptic sampling (Table 2). A constant porosity of 0.39 was used; this porosity value is the same as that used in the analysis of the 1985–1988 test [Garabedian *et al.*, 1991] and agrees with measurements and estimates of porosity in this aquifer [Garabedian *et al.*, 1988; Wolf *et al.*, 1991]. The normalized Ni and Br masses are plotted against the number of days from injection (Figure 6a). No discernible temporal trends were observed. The normalized Br masses for 1993–1994 (Figure 6a) ranged from 0.90 to 1.19, with an average of 1.03 ($n = 8$; injection mass also shown). This average of nearly unity supports the assumptions that Br traveled conservatively and that an average porosity of 0.39 is reasonable for this aquifer. The deviations of estimated Br mass from the injected mass most likely derive from the discontinuous nature of the spatial sampling and the integration approximations required in the spatial moments analysis.

[25] The relative Ni masses (Figure 6a) are on average 0.86 ($n = 8$); about 14% of the Ni mass was adsorbed onto the aquifer sediments at any time during the test. The apparently consistent loss in aqueous Ni suggests that, in general, NiEDTA reversibly adsorbed onto and then desorbed from the aquifer sediments, in agreement with the breakthrough curve results.

3.2.2. Center of mass

[26] The first moment quantifies the location of the center of mass of the tracer cloud. The linear relationship of distance traveled to time in the aquifer for the tracer clouds is shown in Figure 6b. A linear regression applied to the 1993–1994 Br relationship yields a velocity estimate of 0.47 m/d. The scatter around the regression line is small and the correlation coefficient of the relation is high ($r = 0.99$, $n = 9$), implying that the velocity was constant throughout the test. This average Br velocity is similar to the median velocity of 0.46 m/d observed for Br at the breakthrough MLS (Figure 5b).

[27] The relationship between the travel distance and the number of days from injection for Ni (Figure 6b) is nearly linear ($r = 0.99$, $n = 10$); if linearity is assumed, a velocity of 0.39 m/d is calculated. This velocity is lower than that for Br, and is consistent with reversible adsorption of NiEDTA onto the aquifer sediments. The retardation factor of 1.2, calculated from the Ni and Br velocities, is similar to the retardation factors calculated from the breakthrough curves (Figure 5c) and is consistent with a fractional adsorption of 16%, if a linear adsorption isotherm is assumed [Kohler *et al.*, 1996]. This calculated adsorbed mass is similar to the

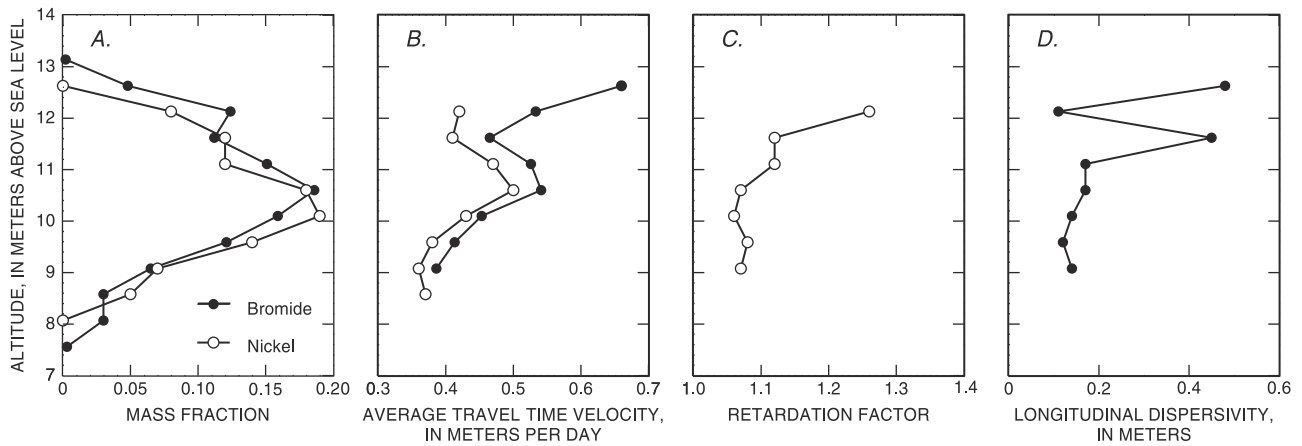


Figure 5. Temporal moments calculated for breakthrough curves at a multilevel sampler (BT2) located 52 m downgradient of the injection: (a) spatial mass fraction for bromide and nickel; (b) average travel time velocity for bromide and nickel; (c) retardation factor of nickel transport relative to bromide transport; (d) longitudinal dispersivity for bromide.

14% estimated from the zeroth moment calculations on the synoptic data. The retardation of nickel relative to bromide is illustrated in a map view of the positions of the centers of mass for the two tracer clouds (Figure 7). By 237 days, the distance between the centers of mass was about 20 m, or about 20% of the distance traveled.

[28] The overall Ni velocity of 0.39 m/d assumes a linear relationship between distance and travel time. Careful inspection of Figure 6b reveals a slight nonlinearity in the trend. Significantly different slopes are obtained through regression analysis of the first five spatial sampling results (0.43 m/d for 0–111 days, $r = 0.97$) and the last five (0.35 m/d for 146–237 days, $r = 0.99$). The Ni tracer cloud slowed with time, indicating that nonlinear adsorption occurred. This nonlinearity was not revealed in the mass calculations. Nonlinear adsorption is discussed further in sections 3.4 and 4.

[29] The map of the centers of mass (Figure 7) shows that the tracer clouds generally followed a flow path toward the southeast, but the trajectory was curved. The calculated direction of the water table gradient at 237 days was 14.5° different than that at 48 days (Figure 7 and Table 2). This is generally consistent with the observed trajectory of the centers of mass. The incremental trajectories between each spatial sampling of the Br cloud are, however, consistently 2 to 6 degrees more to the south than the calculated direction of the water table gradient (Table 2). This consistent difference in horizontal trajectories may be evidence of horizontal anisotropy in the spatial distribution of hydraulic conductivity, an anisotropy which has not been resolved with laboratory and field measurements of hydraulic conductivity [Wolf *et al.*, 1991; Hess *et al.*, 1992]. The difference also may have resulted from undetermined surveying errors in the altitudes of the wells used in the gradient calculations.

[30] The vertical location of the center of mass of both tracers (Figure 6c) shows downward movement of the tracer clouds over the first 111 days. A primary cause of the observed decline in altitude of the center of mass was the greater density of the tracer solution relative to the native groundwater. As the tracer cloud became diluted over time through dispersion, the density contrast diminished and the sinking of the tracers due to this contrast consequently diminished.

[31] Seasonal changes in hydrologic conditions also influenced the vertical trajectory of the tracer cloud. The vertical hydraulic gradients are too small to be detected in this section of the aquifer away from surface discharge boundaries, such as Ashumet Pond, which is about 350 m downgradient from the site (Figure 1). A seasonal pattern in vertical hydraulic gradient is consistent, however, with other observed changes in hydrologic conditions. The 1993 injection was during April when recharge to the aquifer from precipitation usually occurs [Barlow and Hess, 1993]. This recharge creates a downward vertical hydraulic gradient that may be smaller than standard field methods can detect. By July (100 days later), potential evapotranspiration is usually high enough to exceed precipitation, which minimizes recharge to the aquifer and reduces the vertical hydraulic gradient. These seasonal changes in recharge most likely affected the vertical trajectory of the tracer cloud in addition to the effects of density.

[32] In general, the Ni center of mass was slightly lower than the Br center (Figure 6c) for the 1993–1994 test. This consistent difference probably reflected the greater degree of adsorption of NiEDTA in the upper pristine zone because of the lower pH and lack of competition from adsorbing anions, such as phosphate, in the pristine zone than in the contaminated zone.

3.2.3. Variance calculations and dispersivity estimates

[33] The variance tensor (second central moment) is a measure of the spread of the tracer around the calculated center of mass (first moment). The variances can be resolved into three principal components that are roughly aligned with the longitudinal, transverse horizontal, and transverse vertical directions. Dispersivity can be calculated as one half the slope of the linear spatial trend in variance when the velocity is constant throughout the test, as was observed generally here (Figure 6b).

[34] The tracer clouds lengthened with time as they traveled downgradient through the aquifer (Table 1 and Figures 2 and 3). The lengthening is quantified in a monotonic increase in the longitudinal variance with distance traveled (Table 2 and Figure 8a). The increase in Br longitudinal variance was not constant; the trend in the

Table 2. Moment Analysis Results of the Spatial Distribution of the Nonreactive Tracer Bromide and the Reactive Tracer Nickel, Cape Cod, Massachusetts, 1993–1994

Time From Injection, days	Mass, g	Normalized Mass	Location of Center of Mass, m			Cumulative Incremental Distance, m	Incremental Travel Trajectory, ^c deg	Water table Gradient, ^c deg	Principal Components of Variance, m ²			Tracer Cloud Orientation, deg	
			X ^a	Y ^a	Z ^b				Longitudinal	Transverse		Horizontal ^c	Vertical ^d
										Horizontal	Vertical		
<i>Bromide</i>													
0	2708	1.00	0.00	0.00	12.20	0.00	161.0	–	–	–	–	–	–
13	3081	1.14	–0.88	6.20	11.72	6.28	159.7	164.2	1.95	0.77	151.5	–	–13.7
48	2959	1.09	–3.06	23.20	10.83	23.54	159.8	165.0	1.47	0.82	164.5	–	–9.4
83	2871	1.06	–5.23	40.65	10.42	41.03	159.3	165.1	2.27	0.87	164.3	–	–7.4
111	2545	0.94	–6.26	53.17	10.30	53.59	160.4	167.6	2.94	0.79	165.1	–	–5.2
146	2432	0.90	–7.92	68.68	10.16	69.19	162.9	166.2	2.25	0.88	164.0	–	–4.5
175	2434	0.90	–8.48	81.41	10.28	81.94	165.6	169.7	2.62	0.86	164.1	–	–3.1
210	2684	0.99	–8.43	95.89	10.16	96.42	169.4	172.5	3.84	0.79	164.5	–	–2.4
237	3213	1.19	–7.56	108.1	10.08	108.7	174.4	176.3	5.06	0.61	164.2	–	–2.5
<i>Nickel</i>													
0	2530	1.00	0.00	0.00	12.20	0.00	161.0	–	–	–	–	–	–
13	2443	0.97	–0.81	5.51	11.75	5.59	159.7	163.9	1.72	1.05	145.6	–	–4.24
48	2283	0.90	–2.81	21.00	10.72	21.24	159.8	164.9	1.52	1.06	163.0	–	–5.70
83	1987	0.78	–4.65	35.85	10.31	36.21	159.3	165.2	2.01	1.26	161.8	–	–1.46
111	2253	0.89	–5.63	47.17	10.14	47.57	160.4	167.3	2.96	1.35	166.5	–	–1.32
146	1933	0.76	–6.79	60.78	10.15	61.23	162.9	167.4	2.40	1.23	165.2	–	–1.09
175	2283	0.90	–7.14	71.28	10.15	71.74	165.6	170.4	3.10	1.63	164.9	–	–1.40
210	2166	0.86	–7.02	82.89	10.02	83.35	169.4	172.9	3.32	1.09	165.9	–	–0.62
237	2316	0.92	–6.30	91.81	9.86	92.30	174.4	176.9	4.16	1.03	165.0	–	–1.57
314	2362	0.93	–3.88	119.3	9.49	119.9	171.1	177.3	4.99	0.81	165.7	–	–2.09

^aMapped locations are relative to a local coordinate system (Figure 2) aligned with the primary direction of transport (rotated 187.725° relative to magnetic north) observed in the previous tracer test [Garabedian *et al.*, 1991; LeBlanc *et al.*, 1991] and centered on the injection of this test.

^bVertical locations are relative to mean sea level.

^cMapped angles are in degrees east of magnetic north.

^dVertical angles are clockwise from horizontal within the plane defined by the principal axes of the longitudinal and vertical variances.

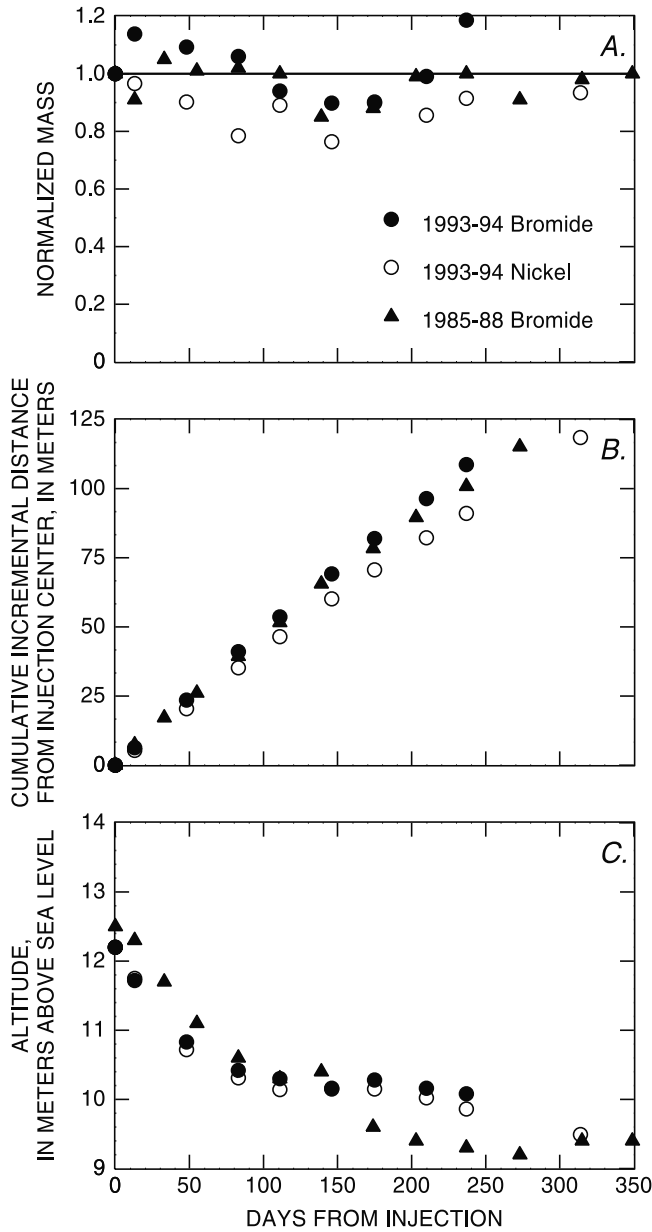


Figure 6. Spatial moments of bromide and nickel tracer clouds calculated for each synoptic sampling: (a) mass (zeroth moment) normalized by the injected mass; (b) cumulative incremental distance from the center of the injection to the center of mass (first moment); (c) calculated altitude of the center of mass (first moment).

variance changed after about 69 m of transport. The longitudinal Br variance increased at a slow rate early in the test. Spatial analysis of the later results (69 to 109 m) shows a larger rate of increase. A linear trend fit to these later time variances yields a longitudinal dispersivity estimate for Br of 2.2 m (Table 3). The correlation coefficient of this linear trend is high ($r = 0.99$). But the number of observations is low ($n = 4$), scatter around the trend is apparent, and the dispersive process may not have reached a constant asymptotic value of longitudinal dispersivity.

[35] The calculated angle of the principal axis of the variance matrix (Table 2) remains fairly constant (161.8 to 165.9° relative to magnetic north) after the first synoptic

sampling. This constant orientation is in contrast to the incremental direction of transport, which tracked increasingly to the south with time as the direction of the water table gradient changed. Differences of as much as 12 degrees were observed between the horizontal cloud orientations and the incremental trajectories (Table 2). The large differences occurred mostly later in the test as the gradient direction changed; the differences in cloud orientations and trajectories may reflect an imprint of earlier trajectories on the distribution of tracers. These differences also may result from the anisotropic hydraulic-conductivity tensor not being aligned with the direction of transport in the aquifer. The longitudinal cloud orientations observed in the first synoptic sampling round were different and prob-

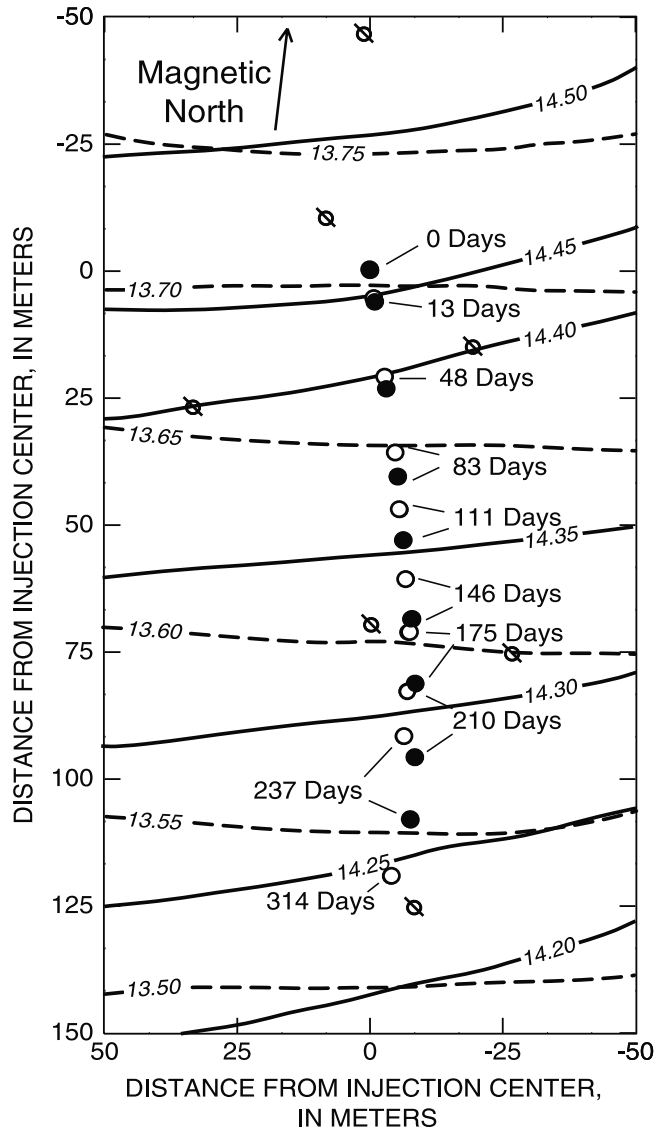


Figure 7. Calculated location of the center of mass (first moment) of bromide (solid circles) and nickel (open circles) for each synoptic sampling round. Water table contours shown for 48 (solid lines) and 237 (dashed lines) days after injection. Locations of only 7 of the 25 observation wells from which water level data were collected are shown (slashed open circles); others are located outside the shown area.

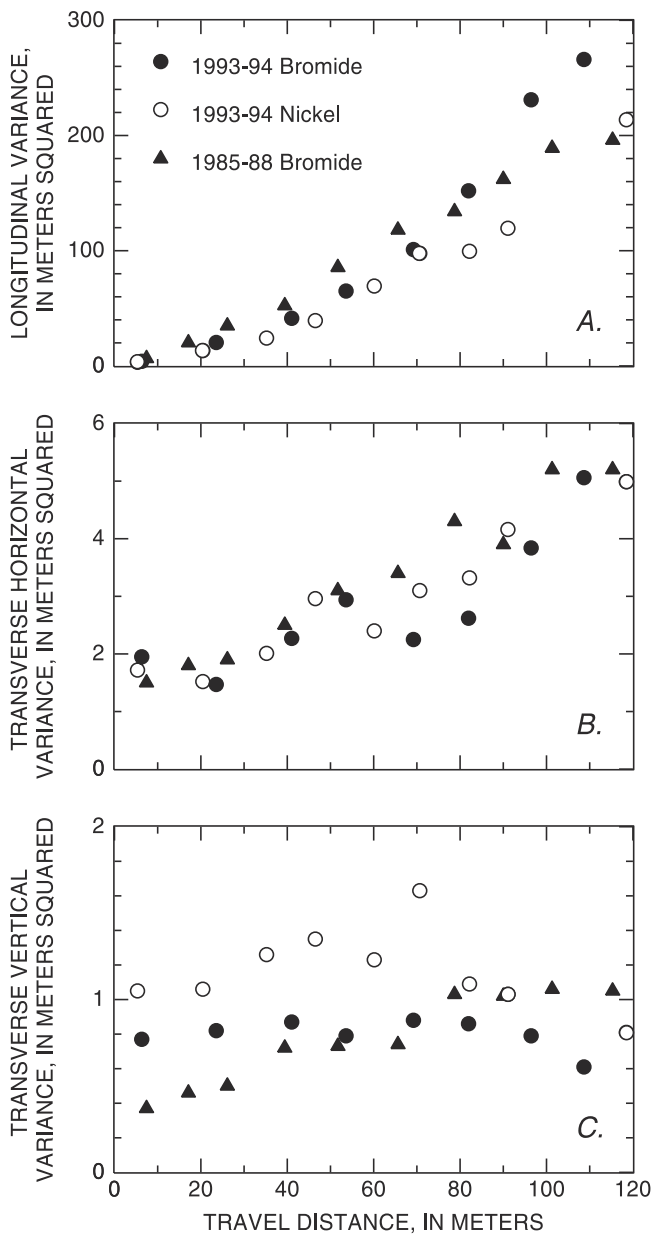


Figure 8. Calculated variances (second central moments) of the bromide and nickel tracer clouds for each synoptic sampling round: (a) longitudinal; (b) transverse horizontal; (c) transverse vertical.

ably reflect local heterogeneities within the aquifer in the vicinity of the injection ports and the configuration of the injection; by design, the tracer clouds were initially larger in the directions transverse to the flow direction than in the longitudinal direction (Table 1).

[36] The change in longitudinal variance for Ni reached a constant value sooner than Br, after a travel distance of about 48 m. The late time linear relationship yielded a dispersivity of 1.1 m ($n = 6$, $r = 0.97$), which is lower than the 2.2 m calculated for Br (Table 3). Possible reasons for the lower dispersivity of Ni relative to Br include: 1) a higher relative detection limit, 2) nonlinear adsorption of NiEDTA, 3) metal exchange between NiEDTA and Fe(III), and 4) spatially variable adsorption of NiEDTA.

[37] The Ni cloud would appear smaller than the Br cloud if more of its mass at the edge of the cloud was unquantified. The method detection limits for Ni and Br, relative to the injected concentrations, are 2×10^{-3} and 0.9×10^{-3} , respectively. These limits are not drastically different, but may account in part for the differences in longitudinal dispersivities.

[38] In the dispersion process, the edge of a tracer cloud mixes with ambient groundwater; tracer concentrations at the edge decrease and the cloud spreads. Adsorption counteracts the dispersion of the tracers. As concentrations decrease, the fraction of NiEDTA that is adsorbed onto the oxyhydroxide coatings increases [Nowack and Sigg, 1996]. An increase in fractional adsorption at lower concentrations may be partly responsible for the smaller longitudinal dispersivity calculated for Ni relative to Br.

[39] At low concentrations of NiEDTA, the exchange reaction with Fe(III) is thermodynamically favored [Davis *et al.*, 2000, 2001b]. Through a series of reaction steps at the solid surface after the NiEDTA complex has adsorbed [Nowack and Sigg, 1996, 1997], the Fe(III) on the solid surface complexes with the EDTA and the Ni ion is freed; the Ni ion then sorbs strongly to the aquifer sediments at the pH range of the groundwater in this experiment; finally, the Fe(III)EDTA complex detaches from the solid surface and is transported with the groundwater. The constancy in the mass of aqueous Ni throughout the test (Figure 6a), however, indicates that the magnitude of this process never was great; otherwise, a loss in mass with time would have been observed. Removal of small amounts of Ni at the edges of the tracer cloud would minimally affect the calculated mass, but could affect noticeably the calculated variances, which are most sensitive to the distribution of tracer at the extreme edges of the tracer cloud.

[40] Adsorption of NiEDTA varied vertically in the aquifer due to the chemical zones formed by the sewage contamination. Adsorption was greatest in the pristine zone (Figure 4). The local velocity in this zone was greater than in the contaminated zone, as reflected in the skewed vertical distribution of Br that formed with time (Figure 3). This greater velocity in the pristine zones resulted from physical heterogeneity and is unrelated to the processes controlling adsorption of Ni. As a consequence, the smaller overall longitudinal dispersion of Ni may have resulted from greater adsorption occurring in the zone where the velocity, by chance, was greatest. Section 3.4 explores further the effects of the large-scale chemical variations on dispersion and reports the results of spatial moments calculated within specific chemical zones.

[41] In general, the transverse horizontal variance of the Br tracer cloud increased with distance (Figure 8b and Table

Table 3. Transport Parameters Estimated From Tests Conducted in 1985–1988 [Garabedian *et al.*, 1991], and 1993–1994 (This Study), Cape Cod, Massachusetts

Parameter	1985–1988 Bromide	1993–1994	
		Bromide	Nickel
Velocity, m/d	0.42	0.47	0.39
Longitudinal dispersivity, m	0.96	2.2	1.1
Transverse horizontal dispersivity, cm	1.8	1.4	1.5
Transverse vertical dispersivity, mm	1.5	0.5	3.8

2). A linear fit ($n = 8$, $r = 0.84$) to these data estimates transverse horizontal dispersivity (one half the slope of the linear relation) as 1.4 cm. If only the later results are included ($n = 4$, $r = 0.98$), as was done with the longitudinal dispersivity calculation, the resulting estimate of transverse horizontal dispersivity for Br is higher (3.6 cm), but within the same order of magnitude as the estimate from the entire set of transverse horizontal variances. This greater late time transverse horizontal dispersion may result from the shift in gradient direction later in the test and the resulting difference between the cloud orientation and the gradient direction [Rehfeldt and Gelhar, 1992; Goode and Konikow, 1990]. Both estimates for transverse horizontal dispersivity are approximately 2 orders of magnitude smaller than the estimate of longitudinal dispersivity.

[42] Transverse horizontal variances for Ni displayed a similar trend with travel distance as Br (Figure 8b). A linear trend through the variances yielded an estimate of transverse horizontal dispersivity of 1.5 cm ($n = 9$, $r = 0.95$), which is essentially equal to the dispersivity calculated for Br (Table 3). If adsorption of NiEDTA and Ni increase as concentrations decrease, as was discussed above, then the transverse horizontal dispersivity for Ni should be less than that for Br. The fact that the two are essentially the same likely reflects the lack of resolution in the sampling network in the transverse horizontal direction (Figure 2).

[43] The transverse vertical variance for Ni was slightly larger than that for Br throughout the test (Figure 8c and Table 2). This slight difference probably reflected the more symmetrical nature of the Ni tracer cloud as compared to the Br cloud (Figure 3). Both tracer clouds showed an increase in vertical variance with travel distance at distances less than 50 m. Initially, the transverse vertical variances increased with distance, resulting in estimates of vertical dispersivity of 0.5 ($n = 6$, $r = 0.68$) and 3.8 mm ($n = 6$, $r = 0.84$) for Br and Ni, respectively. Later, a decreasing trend in transverse vertical variance indicated a slight decrease in the vertical extents of the tracer clouds with travel distance. The decline in the Ni variance could be caused by increased adsorption of Ni at the cloud edges where concentrations are low. However, the Br variance shows a similar decline. An apparent decrease in the vertical extent could have occurred as the outer portion of each tracer cloud decreased to concentrations below the analytical detection limit, or as the cloud moved to areas where the vertical spacing of the sampling network increased (Figure 3). A real decrease in the vertical extent could have occurred if hydraulic changes caused flow to converge into a faster zone or if the cloud became skewed significantly in the vertical transport plane. Regardless of the cause, the calculated decrease in vertical variance was not great in the later part of the test, just as the vertical spread of each cloud earlier in the test was not great, and the estimated transverse vertical values are 1 to 2 orders of magnitude smaller than the transverse horizontal dispersivity.

3.3. Comparison to 1985–1988 Tracer Test

[44] The primary purpose of the 1985–1988 tracer test was to investigate the macrodispersion of a nonreactive anion (Br) as it traveled through the moderately heterogeneous aquifer [LeBlanc et al., 1991; Garabedian et al., 1991]. The sections of aquifer traversed in the 1985–1988

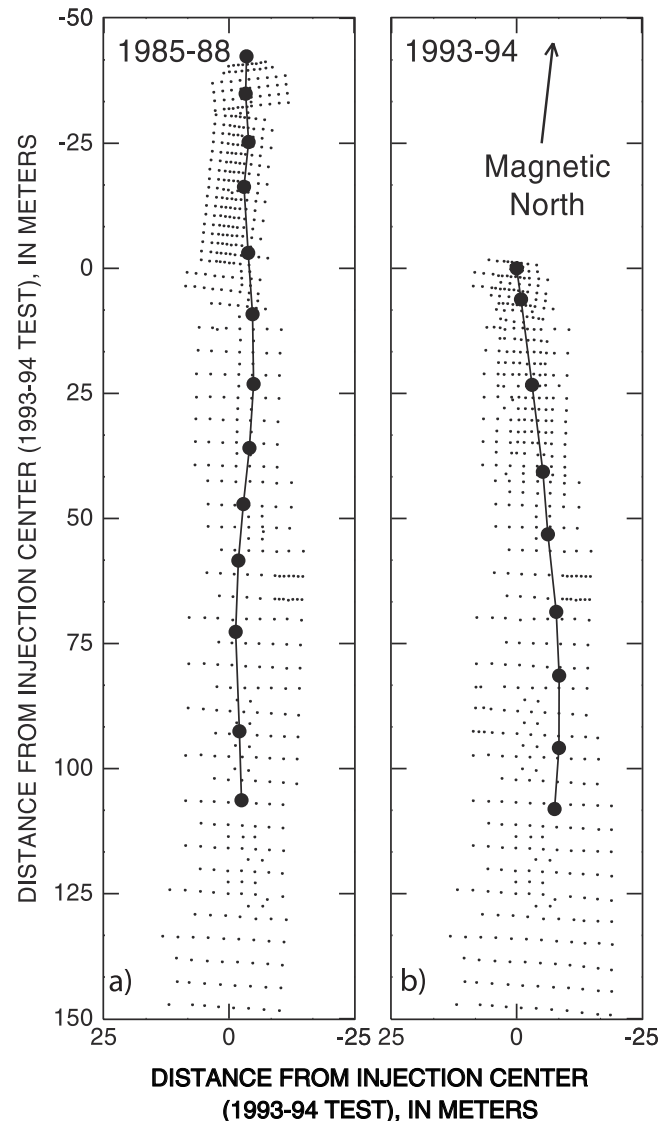


Figure 9. Calculated location of the center of mass (first moment) of bromide for each synoptic sampling round: (a) 1985–1988 experiment [Garabedian et al., 1991] and (b) 1993–1994 experiment. Also shown are the multilevel samplers available for sampling in each experiment.

test and the 1993–1994 test were different, but there was some spatial overlap (Figure 9). Consequently, the spatial stationarity of physical transport properties in this aquifer and the reproducibility of this type of large-scale field experiment can be investigated through a comparison of the results of the two tests.

[45] The distributions of Br in both tests were well characterized by the synoptic sampling rounds and spatial moments analyses. The average normalized masses are not significantly different from unity (Figure 6a). This similarity in characterizing Br mass is encouraging because the instrumentation networks were different in the two tests (Figure 9). The size of the Br tracer cloud was large relative to the horizontal spacing between MLS in the earlier test, as quantified by the ratio of the area of the Br tracer cloud, represented by the product of the square root of the horizontal variances, to the average triangle area used in the

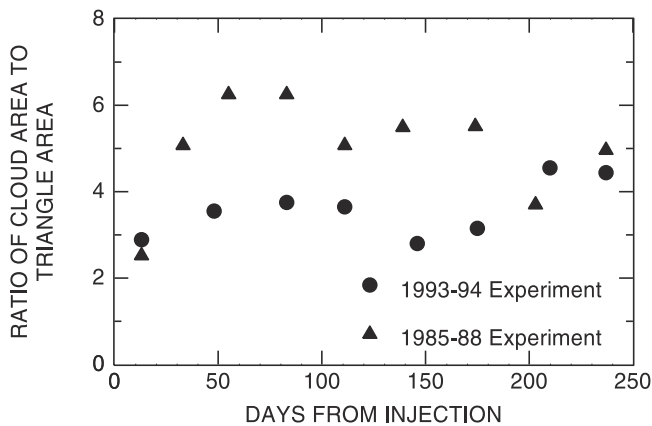


Figure 10. Ratio of the bromide tracer cloud area, represented by the product of the longitudinal and transverse horizontal variances (second central moments), to the average horizontal spacing between sampling points, represented by the average size of the triangles formed among adjacent sampling points and used in the spatial moment analysis, for each synoptic sampling round for the 1985–1988 [Garabedian *et al.*, 1991] and 1993–1994 experiments.

triangular integration step of the spatial moments analysis (Figure 10). In general, this ratio was larger in the 1985–1988 test than in the 1993–1994 test, suggesting that the horizontal resolution of the tracer cloud should have been better in the 1985–1988 test than in the 1993–1994 test. This difference in resolution, however, is not reflected in the Br mass calculations (Figure 6a).

[46] The relationship between distance traveled and time is linear for the Br cloud in each of the two tests (Figure 6b). The average velocities (slopes of each linear relationship) are slightly different. Garabedian *et al.* [1991] reported a velocity of 0.42 m/d for the 1985–1988 test; the velocity calculated for the 1993–1994 test was 0.47 m/d (Table 3). Assuming that the average hydraulic conductivity was the same for the portions of the aquifer traversed in the two tests, the 12% increase in velocity can be explained by the 12% increase in hydraulic gradient in the 1993–1994 test compared to the 1985–1988 test (Figure 11).

[47] Similar density-dependent transport behavior was observed in the two tests (Figure 6c). Both injection solutions were more dense than the native groundwater. The tracer clouds sank extensively during the first 100 days of transport, probably because of this density contrast. The tracer cloud in the 1985–1988 experiment continued to sink until about 237 days after injection. This longer period of sinking may be attributed to seasonal differences in recharge [Barlow and Hess, 1993]. The 1985–1988 test began in July when recharge was low; in October, 100 days into the test, the recharge was higher [LeBlanc *et al.*, 1991]. The 1993–1994 test began in April when recharge was higher; in July, 100 days into the test, likely recharge was near zero. This difference in recharge patterns could explain the differences in vertical sinking.

[48] A final comparison can be made between the variances and dispersivities calculated from the results of each test. A graphical comparison of Br variances calculated for

each test (Figure 8) shows that more time and travel distance were required in the 1993–1994 test for the transport behavior to reach a steady rate of increase in longitudinal variance. About 69 m of travel distance was required in the 1993–1994 test; the 1985–1988 test reached a constant rate after about 26 m [Garabedian *et al.*, 1991]. This difference in the early time behavior in the longitudinal variances of the nonreactive tracer is perhaps the most significant difference between the two tests. The differences in spatial sampling density (Figure 10) may have contributed to this apparent difference in early time behavior. Otherwise, spatial heterogeneity may explain the difference.

[49] The plots of transverse horizontal variance with travel distance for the two tests (Figure 8b) show similar trends with travel distance. This similarity may be real or may reflect a poor resolution of both Br tracer clouds in the transverse horizontal direction considering the size of the tracer clouds and the lateral spacing between MLS.

[50] The transverse vertical variance in the 1993–1994 test showed a different trend from the small, but steady increase (Figure 8c) calculated for the 1985–1988 test [Garabedian *et al.*, 1991]. This difference in calculated Br variances may result from differences in the average vertical spacing between sampling ports. In the earlier test, the tracer cloud traveled through the northern section of the array of MLS (Figure 9) where sampling ports are separated by 25 cm vertically; the sampling ports in the vicinity of the 1993–1994 injection are typically 38 to 46 cm apart. Overall, results from both tests indicated that the Br tracer clouds spread little in the transverse vertical direction.

[51] The overall similarities in the Br variance trends of the tracer tests are reflected in the resulting dispersivities (Table 3). The relative magnitudes of the three dispersivities are the same in the two tests: the longitudinal dispersivity was 2 orders of magnitude greater than the transverse horizontal dispersivity, which was 1 to 2 orders of magnitude greater than the transverse vertical dispersivity. The asymptotic longitudinal dispersivity was twice as great in the 1993–1994 test (2.2 m) as in the 1985–1988 test (0.96 m), but was remarkably similar considering that dispersivity can range over many orders of magnitude [Gelhar *et al.*, 1992]. The transverse horizontal and transverse vertical

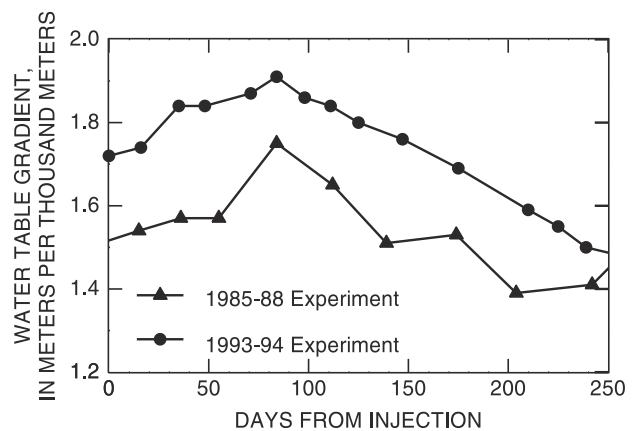


Figure 11. Magnitude of the water table gradient in the vicinity of each tracer test.

dispersivities also were essentially the same for the two tests (Table 3).

[52] The longitudinal dispersivity result of the 1993–1994 test (2.2 m) confirmed the 1985–1988 result (0.96 m). Because the two tests were run in different, but overlapping portions of the aquifer, the similarity of the results suggests spatial stationarity within the dispersive properties of the aquifer; an aquifer transport property is said to be spatially stationary when it is statistically the same throughout the aquifer. The confirmation of spatial stationarity is important for an earlier comparison made by *Hess et al.* [1992] between the results of the 1985–1988 tracer test and the statistical distribution of hydraulic conductivity within the aquifer. The longitudinal dispersivity of 0.78 m calculated from the hydraulic-conductivity distribution, by use of the stochastic transport theory of *Gelhar and Axness* [1983], compares favorably with the dispersivity of 0.96 m that resulted from the 1985–1988 tracer test [*Garabedian et al.*, 1991]. All measurements of hydraulic conductivity were made outside the tracer test array, approximately 15 m to the west [see *Hess et al.*, 1992, Figure 1]. If the distribution of transport properties was not stationary, the comparison made by *Hess et al.* [1992] would be invalid because of the spatial separation of the hydraulic-conductivity measurements and the tracer test array.

3.4. Zoned Moments

[53] The tracers injected in 1993–1994 vertically spanned the three chemical zones in the sewage-contaminated aquifer. The vertical trajectory of the center of mass for both Br and Ni is shown in Figure 12 superimposed on the vertical distribution of the transition zone, as defined by an elevated background concentration of dissolved zinc [*Kent et al.*, 2000]. The center of mass eventually dropped below the defined transition zone. The time and distance trends (Figures 6c and 12) suggest that the proportion of the tracer clouds in each chemical zone varied with time, although the vertical extent of the tracer clouds throughout the test spanned the pristine, transition, and contaminated zones. The temporal variability in the proportion of the tracer

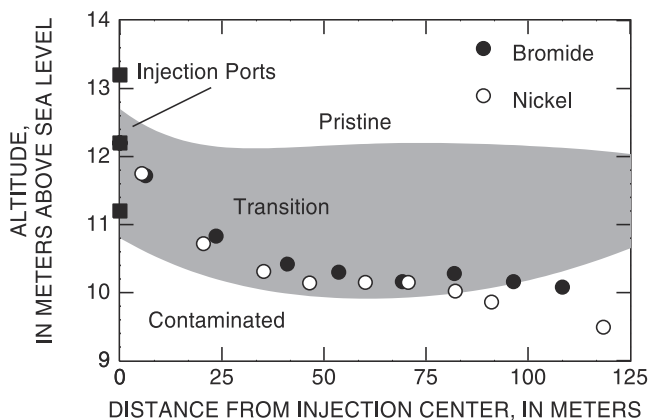


Figure 12. Altitude of the center of mass (first moment) of the bromide and nickel tracer clouds calculated for each synoptic sampling round as a function of cumulative distance from the center of injection. The transition zone was defined based on background zinc concentrations.

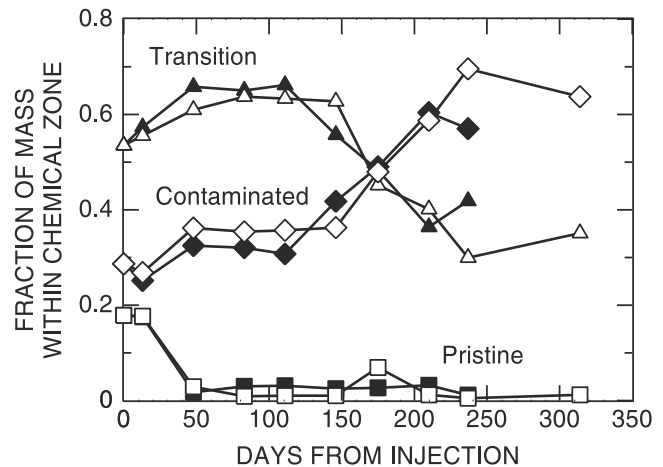


Figure 13. Mass (zeroth moment) of bromide (solid symbols) and nickel (open symbols) tracers calculated for each synoptic sampling round for the pristine, transition, and contaminated chemical zones.

clouds in each chemical zone complicates a quantitative analysis of reactive transport processes observed in this test [see *Davis et al.*, 2000, 2001a, 2001b].

[54] The spatial data were further analyzed to examine the effects of the large-scale variability in chemical conditions in the aquifer. Each spatial data set was divided vertically into pristine, transition, and contaminated zones and spatial moments were calculated on these subsets. The zeroth moment quantifies the tracer mass in each zone at each spatial sampling. The amount of mass in each zone changed with time partly because of the vertical movement of the tracer clouds across the zones. This vertical movement complicates the rigorous evaluation of the higher moments to yield velocities and dispersivities for each chemical zone. However, the resulting higher moments elucidate the geochemical processes affecting the transport of Ni.

3.4.1. Calculated mass

[55] Initially, approximately half of the tracer mass was in the transition zone (53.5%). Significant tracer mass also was injected into the pristine (17.8%) and contaminated (28.7%) zones. Mass in the pristine zone dropped quickly to less than 5% (Figure 13) as the tracer cloud sank across the chemical gradients. In general, the fraction of Ni remaining in the pristine zone was less than that for Br, reflecting the reversible adsorption of Ni in the pristine zone. With time and further sinking of the tracer clouds, the transition zone lost mass and the contaminated zone gained mass.

[56] The vertical distribution of Br and Ni masses within each chemical zone tracked similarly throughout much of the test (Figure 13). The exception was for the final Br sampling at 237 days, at which point the Br mass in the transition zone increased and the mass in the contaminated zone decreased, whereas the Ni mass continued the trend of decreasing mass in the transition zone and increasing mass in the contaminated zone. This deviation resulted from a rise in the boundary between the transition and contaminated zones at a travel distance of about 120 m (see Figure 12). This rise was an artifact of the method used to delineate the zones based on background zinc concentrations. Because Ni significantly lagged behind Br, the effect of this spatial

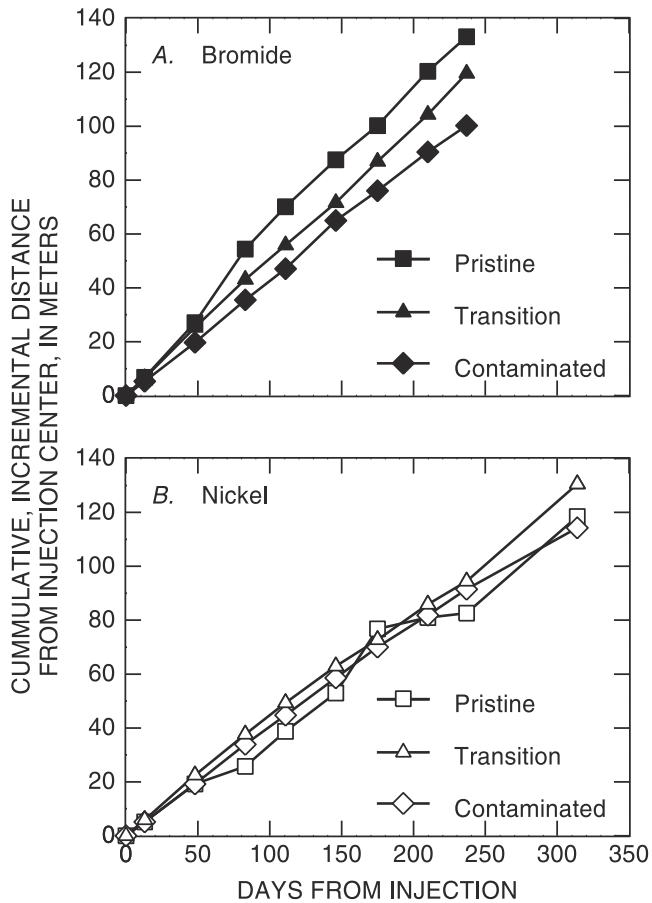


Figure 14. Distance from the center of injection to the center of mass (first moment) calculated for each synoptic sampling round for each chemical zone: (a) bromide and (b) nickel.

change in the boundary between the transition and contaminated zones did not affect the spatial distribution of Ni until the sampling at 314 days (Figure 13).

3.4.2. Center of mass

[57] The first spatial moment of Br, the location of the center of mass, defines different flow velocities in the three zones (Figure 14a), with a decreasing trend in velocity with depth in the aquifer. This trend agrees with the asymmetric shape of the Br cloud that developed early in the test (Figure 3). The differences in Br velocities are due to physical heterogeneity and not to chemical variability.

[58] The first spatial moment of Ni (Figure 14b) shows a different pattern from Br that reflects both physical and chemical variability. The transport velocities in the pristine and contaminated zones are less than the overall velocity (Figure 6b) and that observed in the transition zone (Figure 14b). The lower transport velocity in the contaminated zone corresponds to the lower flow velocity for Br in the contaminated zone (Figure 14a). The lower transport velocity for Ni in the pristine zone, however, reflects the great amount of adsorption that occurred to overcome the faster flow velocity in this zone, as observed in the Br velocity (Figure 14a).

3.4.3. Longitudinal variance and dispersivity estimates

[59] In general, longitudinal variance increased with time in all three chemical zones (Figure 15), indicating that both

tracers continued to disperse in the direction of transport. Some differences were observed, however.

[60] The smallest increases in longitudinal variance (Figure 15c) and, therefore, the smallest amount of longitudinal dispersion, occurred in the contaminated zone. In the transition and contaminated zones (Figures 15b and 15c), Br dispersed more than Ni, as was observed in the analysis of the entire tracer clouds (Figure 8a). The trend in longitudinal variance in the pristine zone was not as consistent as

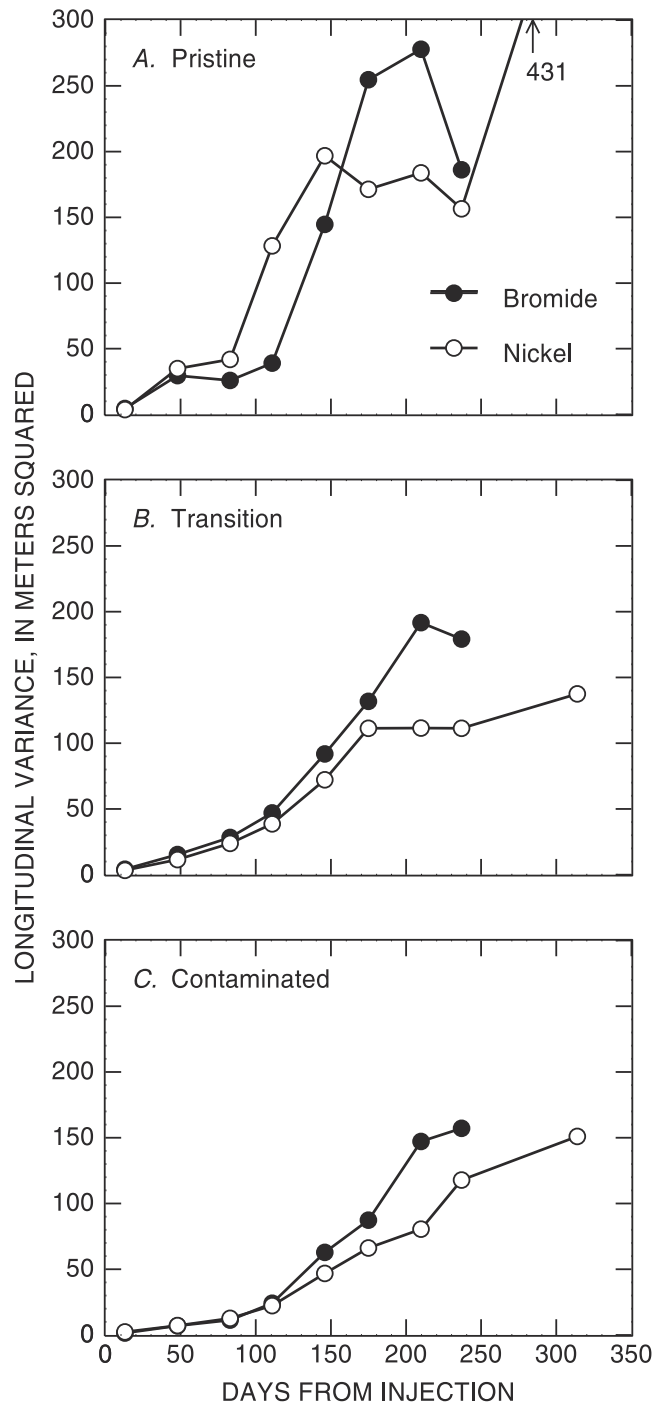


Figure 15. Longitudinal variance (second central moment) calculated for each synoptic sampling round for each chemical zone: (a) pristine; (b) transition; (c) contaminated.

the trends in the other zones (Figure 15a); early in the test, Ni experienced greater dispersion than Br. This trend probably resulted from the reversible adsorption that occurred in the pristine zone. Later, the Br and Ni variance trends cross and longitudinal dispersion in the pristine zone was greater for Br. This later trend may be an artifact of the large errors that most likely dominate the analysis of the tracers in the pristine zone later in the test because so little of the mass remained in the pristine zone (Figure 13).

4. Implications of Observed Dispersion

[61] The smaller overall longitudinal dispersivity calculated for Ni relative to Br was not anticipated. An earlier hypothesis [Garabedian *et al.*, 1988] suggested that a retarded solute could undergo greater dispersion relative to a conservative, nonreactive solute if adsorption was linear and if adsorption properties of the aquifer sediments were negatively correlated with hydraulic conductivity [Robin *et al.*, 1991]. This negative correlation would be expected if adsorption was related to grain size and surface area; smaller grain size and, therefore, larger surface area would result in lower hydraulic conductivity and higher adsorption. A negative correlation between hydraulic conductivity and adsorption could lead to enhanced dispersion by increasing the variation in relative velocities for the reactive solutes. The smaller overall dispersivity for Ni relative to Br suggests the opposite relationship, positive correlation between hydraulic conductivity and adsorption, if the complex reactions controlling Ni transport are neglected.

[62] A simple theoretical model relating adsorption and hydraulic conductivity might be applicable for the transport of solutes that are dominated by cation-exchange reactions with clay minerals; however, few data exist that can be used to quantify this relationship between adsorption and hydraulic conductivity for more complex adsorption processes [Fuller *et al.*, 1996; Tompson and Jackson, 1996], such as may be controlling adsorption of NiEDTA onto the sediments of the Cape Cod aquifer. In coarse-grained, quartz-dominated sediment, adsorption is typically controlled by the hydroxypolymer coatings on mineral surfaces [Coston *et al.*, 1995; Davis *et al.*, 1998]. Consequently, variability in the adsorption of NiEDTA, is probably correlated with variability in the abundance, composition, and reactive surface area of the hydroxypolymer coatings, which does not appear to correlate with overall surface area, and, thus, hydraulic conductivity in these sediments [Fuller *et al.*, 1996; Davis *et al.*, 1993].

[63] Large-scale spatial patterns in adsorption dominate in the Cape Cod aquifer, even if a correlation between hydraulic conductivity and adsorption properties exists. Greater adsorption at the edge of the tracer cloud could occur because concentrations are lower at the edge. This greater adsorption would lead to a sharpening of the tracer cloud edge and a decrease in the spread of the cloud, as has been observed and modeled for the transport of zinc introduced at this site in sewage effluent [Kent *et al.*, 2000]. In addition, increased adsorption at the edge of the tracer cloud may occur because exchange between Fe(III) and Ni in the EDTA complex is more favorable at lower NiEDTA concentrations. This exchange must have been small, if it existed, because there was no quantifiable loss in Ni mass with time (Figure 6a). The enhanced adsorption at

the edge of the tracer cloud may have been significant enough, however, to affect calculated variances.

[64] The basic dispersion theory also does not account for spatial variation in adsorption that may be caused by large-scale variability in background chemical conditions. Brusseau and Srivastava [1999], in an analysis of a reactive tracer used in the 1985–1988 tracer test (not discussed with Br in section 3.3), concluded that the large-scale variability in the background chemical conditions controlled the late time transport behavior of the reactive tracer. The change in the vertical distribution of the tracers through time in the 1993–1994 test (Figure 3) showed greater adsorption of NiEDTA in the pristine zone where pH and competition for adsorption sites were low. Early in the test, greater dispersion of Ni was observed in the pristine zone relative to Br (Figure 15a). This trend, however, was not seen when behavior of the entire tracer clouds was analyzed (Figure 8a). Less dispersion of Ni relative to Br was observed in the transition and contaminated zones (Figures 15b and 15c). The adsorption of Ni depended on the concentrations of Ni and competing ions, the pH, and the coatings on the aquifer sediments. These dependencies likely affected the observed dispersion of the Ni tracer cloud as it traveled through the aquifer.

5. Summary and Conclusions

[65] A large-scale tracer test was conducted in 1993–1994 in an unconfined, sand-and-gravel aquifer on Cape Cod, Massachusetts, to investigate the reactive transport of multiple solute species under spatially variable chemical conditions. A plume of sewage-contaminated groundwater imparts spatially varying chemical conditions in the aquifer, where pH and the concentration of ions competing for adsorption sites increase with depth.

[66] The nonreactive, conservative anionic tracer, bromide (Br), was transported with the flowing groundwater at a constant rate of 0.47 m/d. As expected, the mass of Br throughout the test was estimated to be nearly equal to the mass injected. The dispersivities calculated from the spread of Br with time were 2.2 m, 1.4 cm, and 0.5 mm in the longitudinal, transverse horizontal, and transverse vertical directions, respectively.

[67] The quantitative results of the transport of Br in this experiment are similar to those from an experiment of similar scale that was conducted in 1985–1988 in this aquifer [LeBlanc *et al.*, 1991; Garabedian *et al.*, 1991]. The longitudinal dispersivity is twice as large as that calculated in the 1985–1988 test (0.96 m), but still is remarkably similar considering the many orders of magnitude over which longitudinal dispersivity is observed to range. The transverse horizontal and vertical dispersivities are in the centimeter and millimeter ranges, respectively, as observed in the 1985–1988 test. In both tests, a constant longitudinal dispersivity was achieved for the scale of the experiment; however, the travel distance needed to reach the constant dispersivity differed. In the 1985–1988 test, this occurred over the first 26 m; in the 1993–1994 test, 69 m were required. This difference in early time behavior is the most significant difference in the results of the two Br experiments and suggests a spatial or temporal variability in the early time evolution of groundwater solute plumes.

[68] The 1993–1994 test spatially overlapped a part of the aquifer traversed in the 1985–1988 test. The similarity

of results indicates that dispersion properties are spatially stationary, at least at the combined distance of about 300 m covered in the two tests. The issue of spatial stationarity is important for evaluating the comparison made by *Hess et al.* [1992] between the longitudinal dispersivity calculated from results of the 1985–1988 tracer test and that calculated from a stochastic transport theory applied to the statistical properties of the hydraulic-conductivity distribution in the aquifer. The analysis of the variability in the hydraulic conductivity was done near the tracer test site, within the same aquifer, but off to the side. If spatial stationarity had not been observed, then the comparison made by *Hess et al.* [1992] would not be valid.

[69] About 14% of the injected Ni mass was not observed throughout the test, suggesting reversible adsorption of NiEDTA onto oxyhydroxide coatings on the aquifer sediments. Ni was transported at an average rate of 0.39 m/d, equivalent to a retardation factor of 1.2 relative to the transport of Br. The velocity was not constant; the Ni cloud slowed slightly with time. The calculated longitudinal, transverse horizontal, and transverse vertical dispersivities were 1.1 m, 1.5 cm, and 3.8 mm, respectively.

[70] The overall longitudinal dispersivity for Ni was lower than that calculated for Br. The spatially varying background chemistry resulted in the greatest adsorption of Ni in the pristine zone where groundwater velocities were higher as indicated by the asymmetrical Br distribution. In addition, nonlinear adsorption was expected from laboratory tests and suggested by the slight decrease in velocity. Nonlinear adsorption of NiEDTA would result in greater adsorption at lower concentrations and, therefore, at the edge of the tracer cloud. Each of these factors probably contributed to an overall longitudinal dispersivity for Ni that was smaller than that for Br. When analyzed by chemical zone, Ni showed less dispersion than did Br in the transition and contaminated zones. In the pristine zone overlying the sewage contamination, Ni dispersed more than Br early in the test.

[71] The detailed spatial and temporal data sets collected in this experiment and the initial analysis provided here and in earlier publications [*Davis et al.*, 2000, 2001a, 2001b] offer information needed for testing hypotheses of reactive transport processes under spatially varying chemical conditions. It is our hope that the experimental data will spur further calibration of reactive transport models, coupling the physical transport, speciation, and adsorption processes that control the transport of reactive metals, such as nickel, in the subsurface.

[72] **Acknowledgments.** This project was supported by the Toxic Substances Hydrology Program of the U.S. Geological Survey and the Robert S. Kerr Laboratory of the U.S. Environmental Protection Agency (grant DW14935626).

References

- Barber, L. B., II, E. M. Thurman, and D. D. Runnells, Geochemical heterogeneity in a sand and gravel aquifer: Effect of sediment mineralogy and particle size on the sorption of chlorobenzenes, *J. Contam. Hydrol.*, 9(1), 35–54, 1992.
- Barlow, P. M., and K. M. Hess, Simulated hydrologic responses of the Quashnet River stream-aquifer system to proposed ground-water withdrawals, Cape Cod, Massachusetts, *U.S. Geol. Surv. Water Resour. Invest. Rep.*, 93-4064, 52 pp., 1993.
- Boggs, J. M., S. C. Young, L. M. Beard, L. W. Gelhar, K. R. Rehfeldt, and E. E. Adams, Field study of dispersion in a heterogeneous aquifer, 1, Overview and site description, *Water Resour. Res.*, 28(12), 3281–3291, 1992.
- Brusseau, M. L., and R. Srivastava, Nonideal transport of reactive solutes in heterogeneous porous media, 4, Analysis of the Cape Cod natural-gradient field experiment, *Water Resour. Res.*, 35(4), 1113–1125, 1999.
- Coston, J. A., C. C. Fuller, and J. A. Davis, Pb²⁺ and Zn²⁺ adsorption by a natural aluminum- and iron-bearing surface coating on an aquifer sand, *Geochim. Cosmochim. Acta*, 59(17), 3535–3547, 1995.
- Davis, J. A., C. C. Fuller, J. A. Coston, K. M. Hess, and E. Dixon, Spatial heterogeneity of geochemical and hydrologic parameters affecting metal transport in ground water, *U.S. Environ. Prot. Agency Environ. Res. Brief, EPA/600/S-93/006*, 22 pp., 1993.
- Davis, J. A., J. A. Coston, D. B. Kent, and C. C. Fuller, Application of the surface complexation concept to mineral assemblages, *Environ. Sci. Technol.*, 32, 2820–2828, 1998.
- Davis, J. A., D. B. Kent, J. A. Coston, K. M. Hess, and J. L. Joye, Multi-species reactive tracer test in an aquifer with spatially variable chemical conditions, *Water Resour. Res.*, 36(1), 119–134, 2000.
- Davis, J. A., K. M. Hess, D. B. Kent, J. A. Coston, J. L. Joye, P. Brienens, and K. W. Campo, Multispecies reactive tracer test in a sand and gravel aquifer, Cape Cod, Massachusetts, part 1, Experimental design and transport of bromide and nickel-EDTA tracers, *U.S. Environ. Prot. Agency Environ. Res. Brief, EPA/600/R-01/007a*, 38 pp., 2001a.
- Davis, J. A., J. A. Coston, D. B. Kent, K. M. Hess, J. L. Joye, P. Brienens, and K. W. Campo, Multispecies reactive tracer test in a sand and gravel aquifer, Cape Cod, Massachusetts, part 2, Transport of chromium(VI) and lead-, copper-, and zinc-EDTA tracers, *U.S. Environ. Prot. Agency Environ. Res. Brief, EPA/600/R-01/007b*, 47 pp., 2001b.
- Engesgaard, P., and R. Traberg, Contaminant transport at a waste residue deposit, 2, Geochemical transport modeling, *Water Resour. Res.*, 32(4), 939–951, 1996.
- Fuller, C. C., J. A. Davis, J. A. Coston, and E. Dixon, Characterization of metal adsorption variability in a sand and gravel aquifer, Cape Cod, Massachusetts, U.S.A., *J. Contam. Hydrol.*, 22(3–4), 165–187, 1996.
- Garabedian, S. P., L. W. Gelhar, and M. A. Celia, Large-scale dispersive transport in aquifers: Field experiments and reactive transport theory, *Hydrol. Water Resour. Syst. Rep. 315*, 290 pp., Ralph M. Parsons Lab., Mass. Inst. of Tech., Cambridge, 1988.
- Garabedian, S. P., D. R. LeBlanc, L. W. Gelhar, and M. A. Celia, Large-scale natural-gradient tracer test in sand and gravel, Cape Cod, Massachusetts, 2, Analysis of spatial moments for a nonreactive tracer, *Water Resour. Res.*, 27(5), 911–924, 1991.
- Gelhar, L. W., and C. L. Axness, Three dimensional stochastic analysis of macrodispersion in aquifers, *Water Resour. Res.*, 19(1), 161–180, 1983.
- Gelhar, L. W., C. Welty, and K. R. Rehfeldt, A critical review of data on field-scale dispersion in aquifers, *Water Resour. Res.*, 28(7), 1955–1974, 1992.
- Goode, D. J., and L. F. Konikow, Apparent dispersion in transient ground-water flow, *Water Resour. Res.*, 26(10), 2339–2351, 1990.
- Harvey, R. W., and S. P. Garabedian, Use of colloid filtration theory in modeling movement of bacteria through a contaminated sandy aquifer, *Environ. Sci. Technol.*, 25(1), 178–185, 1991.
- Hess, K. M., S. H. Wolf, and M. A. Celia, Large-scale natural gradient tracer test in sand and gravel, Cape Cod, Massachusetts, 3, Hydraulic-conductivity variability and calculated macrodispersivities, *Water Resour. Res.*, 28(8), 2011–2027, 1992.
- Kent, D. B., J. A. Davis, L. C. D. Anderson, B. A. Rea, and T. D. Waite, Transport of chromium and selenium in the suboxic zone of a shallow aquifer: Influence of redox and adsorption reactions, *Water Resour. Res.*, 30(4), 1099–1114, 1994.
- Kent, D. B., R. H. Abrams, J. A. Davis, J. A. Coston, and D. R. LeBlanc, Modeling the influence of variable pH on the transport of zinc in a contaminated aquifer using semiempirical surface complexation models, *Water Resour. Res.*, 36(12), 3411–3425, 2000.
- Kohler, M., G. P. Curtis, D. B. Kent, and J. A. Davis, Experimental investigation and modeling of uranium(VI) transport under variable chemical conditions, *Water Resour. Res.*, 32(12), 3539–3551, 1996.
- LeBlanc, D. R., Sewage plume in a sand and gravel aquifer, Cape Cod, Massachusetts, *U.S. Geol. Surv. Water Supply Pap.*, 2218, 28 pp., 1984.
- LeBlanc, D. R., and M. A. Celia, Numerical simulation of downward movement of solutes during a natural-gradient tracer test in sand and gravel, Cape Cod, Massachusetts, in *U.S. Geological Survey Toxic Substances Hydrology Program—Proceedings of the Technical Meeting*, edited by D. W. Morganwalp and D. A. Aronson, *U.S. Geol. Surv. Water Resour. Invest. Rep.*, 94-4015, 283–287, 1996.

- LeBlanc, D. R., S. P. Garabedian, K. M. Hess, L. W. Gelhar, R. D. Quadri, K. G. Stollenwerk, and W. W. Wood, Large-scale natural-gradient tracer test in sand and gravel, Cape Cod, Massachusetts, 1, Experimental design and observed tracer movement, *Water Resour. Res.*, 27(5), 895–910, 1991.
- MacIntyre, W. G., M. Boggs, C. P. Antworth, and T. B. Stauffer, Degradation kinetics of aromatic organic solvents introduced into a heterogeneous aquifer, *Water Resour. Res.*, 29(12), 4045–4051, 1993.
- Mackay, D. M., D. L. Freyburg, P. V. Roberts, and J. A. Cherry, A natural gradient experiment on solute transport in a sand aquifer, 1, Approach and overview of plume movement, *Water Resour. Res.*, 22(13), 2017–2029, 1986.
- Masterson, J. P., B. D. Stone, D. A. Walter, and J. Savoie, Hydrogeologic framework of western Cape Cod, Massachusetts, *U.S. Geol. Surv. Hydrol. Invest. Atlas*, HA740, 1 plate, 1997.
- Nowack, B., and L. Sigg, Adsorption of EDTA and metal-EDTA complexes on goethite, *J. Colloid Interface Sci.*, 177, 106–121, 1996.
- Nowack, B., and L. Sigg, Dissolution of Fe(III) (hydr)oxides by metal-EDTA complexes, *Geochim. Cosmochim. Acta*, 61, 951–963, 1997.
- Oldale, R. N., and R. A. Barlow, Geologic map of Cape Cod and the islands, Massachusetts, *U.S. Geol. Surv. Misc. Invest. Rep.*, I-1763, 1 plate, 1986.
- Parkhurst, D. L., User's guide to PHREEQC: A computer program for speciation, reaction-path, advective-transport, and inverse geochemical calculations, *U.S. Geol. Surv. Water Resour. Invest. Rep.*, 95-4227, 143 pp., 1995.
- Rea, B. A., D. B. Kent, D. R. LeBlanc, and J. A. Davis, Mobility of zinc in a sewage-contaminated aquifer, Cape Cod, Massachusetts, in *U.S. Geological Survey Toxic Substances Hydrology Program—Proceedings of the Technical Meeting*, edited by G. E. Mallard and D. A. Aronson, *U.S. Geol. Surv. Water Resour. Invest. Rep.*, 91-4034, 88–95, 1991.
- Rehfeldt, K. R., and L. W. Gelhar, Stochastic analysis of dispersion in unsteady flow in heterogeneous aquifers, *Water Resour. Res.*, 28(8), 1955–1974, 1992.
- Roberts, P. V., M. N. Goltz, and D. M. Mackay, A natural gradient experiment on solute transport in a sand aquifer, 3, Retardation estimates on mass balances for organic solutes, *Water Resour. Res.*, 22(13), 2047–2058, 1986.
- Robin, M. J. L., E. A. Sudicky, R. W. Gillham, and R. G. Kachanoski, Spatial variability of strontium distribution coefficients and their correlation with hydraulic conductivity in the Canadian Forces Base Borden Aquifer, *Water Resour. Res.*, 27(10), 2619–2632, 1991.
- Smith, R. L., B. L. Howes, and S. P. Garabedian, In situ measurement of methane oxidation in groundwater by using natural-gradient tracer tests, *Appl. Environ. Microbiol.*, 57(7), 1997–2004, 1991.
- Stollenwerk, K. G., Modeling the effects of variable groundwater chemistry on adsorption of molybdate, *Water Resour. Res.*, 31(2), 347–357, 1995.
- Tompson, A. F. B., and K. J. Jackson, Reactive transport in heterogeneous systems: An overview, in *Reactive Transport in Porous Media*, edited by C. I. Steefel, P. Lichner, and E. Oelkers, *Rev. Mineral.*, 34, 269–310, 1996.
- Valocchi, A. J., Validity of the local equilibrium assumption for modeling sorbing solute transport through homogeneous soils, *Water Resour. Res.*, 21(6), 808–820, 1985.
- Walter, D. A., B. A. Rea, K. G. Stollenwerk, and J. Savoie, Geochemical and hydrologic controls on phosphorus transport in a sewage-contaminated sand and gravel aquifer near Ashmet Pond, Cape Cod, Massachusetts, *U.S. Geol. Surv. Water Supply Pap.*, 2463, 89 pp., 1996.
- Wolf, S. H., M. A. Celia, and K. M. Hess, Evaluation of hydraulic conductivities calculated from multi-port permeameter measurements, *Ground Water*, 29(4), 516–525, 1991.
- Yeh, G. T., and K. Salvage, HYDROGEOCHEM 2.1: A coupled model of hydrologic transport and geochemistry with both equilibrium and kinetic reactions, technical report, Dep. Of Civ. and Environ. Eng., Pa. State Univ., State College, 1995.
- Zhang, H., F. W. Schwartz, W. W. Wood, S. P. Garabedian, and D. R. LeBlanc, Simulation of variable-density flow and transport of reactive and nonreactive solutes during a tracer test at Cape Cod, Massachusetts, *Water Resour. Res.*, 34(1), 67–82, 1998.

J. A. Coston, J. A. Davis, and D. B. Kent, U.S. Geological Survey, 345 Middlefield Road, Menlo Park, CA 94305, USA.

K. M. Hess, U.S. Geological Survey, 10 Bearfoot Road, Northborough, MA 01532, USA. (kmhess@usgs.gov)